Reports

Direct and Remote Sensing Observations of the Effects of Ships on Clouds

LAWRENCE F. RADKE, JAMES A. COAKLEY, JR., MICHAEL D. KING

Under certain conditions ships can affect the structure of shallow layer clouds. Simultaneous observations of two ship track signatures in stratus clouds from a satellite and in situ from an aircraft show that in the ship tracks the droplet sizes were reduced and total concentrations of both droplets and particles were substantially increased from those in adjacent clouds. In situ measurements of the upwelling radiance within the ship tracks was significantly enhanced at visible wavelengths, whereas radiance at 2.2 micrometers was significantly reduced. Cloud reflectivity along the tracks was enhanced at 0.63 and 3.7 micrometers. These observations support the contention that ship track signatures in clouds are produced primarily by particles emitted from ships.

CONCENTRATIONS OF CLOUD DROPLETS are determined primarily by the concentrations of cloud condensation nuclei (CCN) in the air (*1*). Anthropogenic sources of pollution can affect CCN concentrations (*2*), and CCN from such sources may already have affected clouds on a continental scale (*3*). Increases in CCN may play an important role in climate through their effects on the proportion of solar radiation reflected by clouds (*4*).

An interesting example of the effects of anthropogenic CCN on cloud reflectivity is the so-called "ship track" phenomenon. Ship tracks were first observed in cloudless conditions with satellite imagery under the unusual circumstances when particle emissions from the ship were evidently needed for the formation of a visible cloud (*5*). However, they appear more frequently in satellite imagery as modifications to already existing low-lying stratus and stratocumulus clouds. Tracks are seen most clearly in satellite imagery by comparison of the radiance at 3.7 μm with that at 0.63 or 11 μm (*6*). In order to account for the observed change in radiance, cloud droplet concentrations must be comparatively high and the mean size of the cloud droplets small in the ship tracks.

In this report we describe results of simultaneous measurements from both aircraft and satellites of clouds modified by the emissions from ships. The observations were made in marine stratocumulus clouds during FIRE (*7*) off the coast of southern California on 10 July 1987. The satellite observations, of a pair of roughly parallel ship tracks, were made from the NOAA-10 Advanced Very High Resolution Radiometer (AVHRR) as it passed over the region at 1538 UTC (Fig. 1). The reflectivity at 0.63 μm (Fig. 1A) for the ship tracks (objectively identified) was 68.3 ± 1.4% and that for the noncontaminated clouds was 60.9 ± 4.5% (mean ± SD). The higher reflectivity of the ship tracks was also apparent at 3.7 μm (Fig. 1B). The two ship tracks were penetrated by the University of Washington's C-131A research aircraft between 1556 and 1609 UTC on 10 July 1987 in the vicinity of 32°N and 120°W. The aircraft flew about midway between the top and bottom of the stratocumulus layer, which was about 500 m thick.

The aircraft measurements indicate that distribution of cloud droplet sizes changed dramatically in both ship tracks (Fig. 2). The ship tracks are also evident in measurements of the total concentration of cloud droplets (Fig. 3A) and, unexpectedly, in the cloud liquid-water content (Fig. 3B). These measurements permit estimates of differences in optical depth (τ) and effective cloud droplet radius (r_e), the mean droplet radius as weighted by the droplet cross-sectional area, in the ship tracks and the surrounding cloud unaffected by the ships. The optical depth of a cloud is (*8*)

$$\tau \propto N^{1/3} W^{2/3} \quad (1)$$

where N is the total droplet number concentration and W is the cloud liquid-water content. The aircraft data therefore suggest that τ was enhanced by a factor of 2.6 over that of the noncontaminated cloud in the first ship track and by a factor of 2.1 in each of the two peaks of the second ship track. The effective cloud droplet radius is (*8*)

$$r_e \propto \frac{3W}{2\tau} \quad (2)$$

which can be compared with the value derived from the droplet size distribution. Using Eq. 2, we would predict a negligible reduction of r_e for the first ship track (a factor of 0.96) when compared to the unaffected clouds, but a significant reduction in the second ship track (0.82). Direct measurements show that r_e decreased from 12 to 10.5 μm (88%) in the first track and from 11.2 to 7.5 μm (67%) in the second track. These results emphasize the radiatively important role of the unexpectedly high liquid-

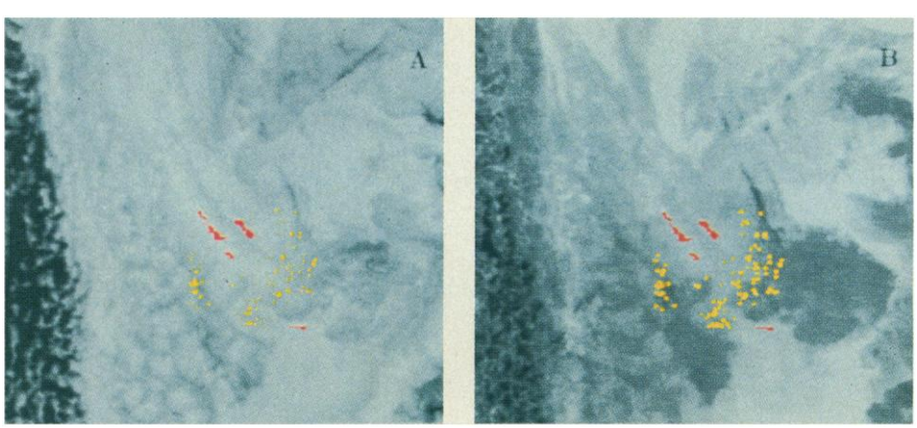

Fig. 1. Images constructed from 1 km by 1 km NOAA-10 AVHRR data at (**A**) 0.63 μm and (**B**) 3.7 μm that contain the ship tracks transected by the C-131A aircraft. The images are for a 200 by 190 km region of ocean off the coast of southern California. Parts of the ship tracks have been identified at both wavelengths by objective analysis (red lines). Randomly selected, noncontaminated cloud pixels are identified by yellow dots.

L. F. Radke, Department of Atmospheric Sciences, University of Washington, Seattle, WA 98195.
J. A. Coakley, Jr., Department of Atmospheric Sciences, Oregon State University, Corvallis, OR 97331.
M. D. King, Laboratory for Atmospheres, National Aeronautics and Space Administration, Goddard Space Flight Center, Greenbelt, MD 20771.

water content and reduced droplet size in the ship tracks.

Airborne measurements of the total concentration of all particles (Aitken nuclei) also showed a sharp increase across the ship tracks (Fig. 3C). These measurements (*9*) were made in the cloud and represent mainly cloud interstitial aerosol (*10*). However, because of the sampling technique, some of these particles are the evaporated residues of cloud droplets. Hence, for incloud measurements, a modest correlation is to be expected between the total concentrations of cloud droplets and particles. The sharp increase in the total concentration of particles in the ship tracks, however, must have resulted from a dramatic increase in the concentration of interstitial particles (that is, particles that did not serve as CCN at the cloud's supersaturation).

The ship tracks can also be seen in the airborne measurements of the upwelling shortwave flux density in the cloud layer, which increased from around 150 to 280 W m^{-2} in the first ship track and to 260 W m^{-2} in the second ship track (Fig. 3D). The downwelling shortwave flux density, on the other hand, showed a modest decrease. These measurements were obtained with broadband Eppley pyranometers mounted on the fuselage of the aircraft. Also aboard the aircraft was a multichannel cloud-absorption radiometer, which measured the angular distribution of scattered radiation at 13 wavelengths between 0.5 and 2.3 μm (*11*). As the aircraft penetrated the two ship-track features, all narrowband channels of the cloud-absorption radiometer showed significant changes. In general, the upwelling (nadir) radiance increased in the shortest (0.5 to 1.03 μm) wavelength channels and decreased in the longest (1.2 to 2.3 μm) wavelength channels. These changes are consistent with the observed increase in the total optical thickness of the cloud layer (*12*) and are a direct consequence of the increase in total concentration of small droplets, while the mean droplet radius decreased (Figs. 2 and 3A). Thus, the increased upwelling flux (Fig. 3D) reflects primarily the increased upwelling radiance at wavelengths less than about 1.0 μm, wavelengths for which the solar radiation is the greatest.

Ship tracks can be identified from satellite images most readily at 3.7 μm (*6*). However, the greater number of spectral channels available from our airborne cloud-absorption radiometer suggest that the radiance ratio between absorbing and nonabsorbing wavelengths can provide a strong signature of ship tracks in clouds (Fig. 3E). For example, both ship tracks are sharply defined by the ratio of the radiance at 0.744 μm to that at 2.20 μm (measured in the cloud) for both the nadir and zenith directions as a function of aircraft flight distance. The first ship track shows an increase in the spectral ratio of about a factor of 20 whereas the second ship track shows an increase of about a factor of 5. These changes in the internal scattered radiation field are thus not confined to the nadir (satellite-viewing) direction, but are reflected in the entire angular distribution of scattered radiation in a cloud.

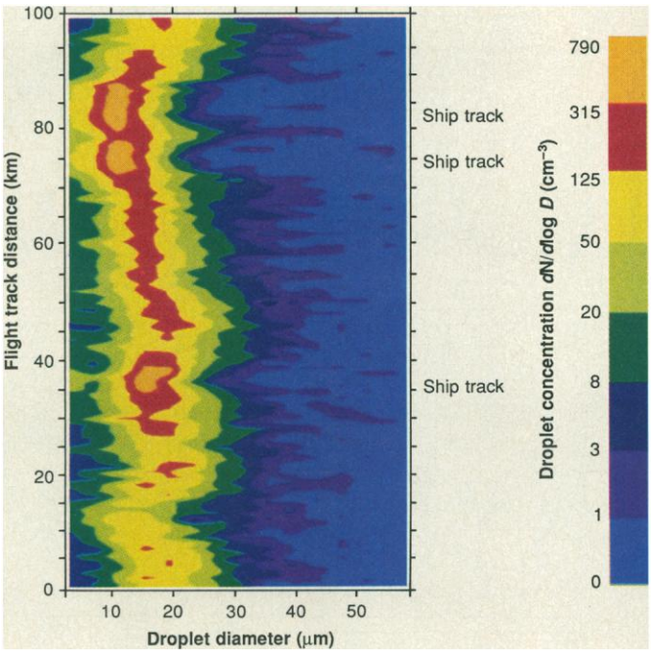

Fig. 2. Size distribution along flight path showing the two ship tracks. The second track had a double peak in the number of droplets. The color scale is logarithmic in order to show the variability found in the noncontaminated part of the cloud.

Could particles produced by the ships modify the clouds as described above? We calculated the flux of CCN that a ship would have to produce to cause the changes in droplet concentrations that we observed. Assuming a ship speed of 10 m s^{-1} and using the measurements of 17 km and ~500 m for the width and depth, respectively, of the second ship track and the measured increase in droplet concentration of 80 cm^{-3} in the track, we find that a ship would have to generate $\sim 2 \times 10^{16}$ CCN per second (*13*) to produce these changes. This flux requires the ship to be a large source of CCN. From the concentrations of interstitial particles in the two ship tracks (Fig. 3C), we calculated that each ship was producing a total flux of particles (Aitken nuclei) of this magnitude.

Subsequent airborne measurements in a cloud-free environment above a large cargo ship showed a total emission flux of 4×10^{15} particles per second. Another large vessel, powered by low rpm marine diesel engines, had a similar emission flux, but simultaneous measurements with a CCN counter (*14*) showed that only ~10% of the particles in the exhaust from this particular ship were CCN. It appears from these measurements that, although ships do emit particles that serve as CCN, they most likely do not directly emit sufficient numbers of CCN to account for the formation of the ship tracks. Laboratory measurements of the ratio of CCN to all particles in fuel oil combustion also support this conclusion (*15*).

The explanation for this discrepancy may partly lie in the conversion of the gases emitted by the engines of ships into particles. Comparatively rapid production of CCN by gas-to-particle conversion in the atmosphere has been observed in power-plant plumes, where this mechanism can dwarf direct particle emissions and can produce phenomena remarkably similar to ship tracks ("stack tracks") in overlying layer clouds (*16*).

One of the remarkable features of ship tracks is their persistence. If all of the CCN necessary to modify the cloud were delivered in an initial pulse at cloud base and then were subsequently spread by dilution, the average cloud droplet size would be smallest and the droplet concentration would be highest at the head of the track (hence optically brightest). Subsequent dilution of the CCN would rapidly reduce their effect on the cloud. However, ship tracks are not markedly brighter at their head, nor do they monotonically decrease in brightness along the track. Hence, there is apparently continual production of CCN in the track, such as would be provided by gas-to-particle conversion.

Our airborne measurements also suggest that there was an evolutionary transformation of the particles (Fig. 3, A and C) in the

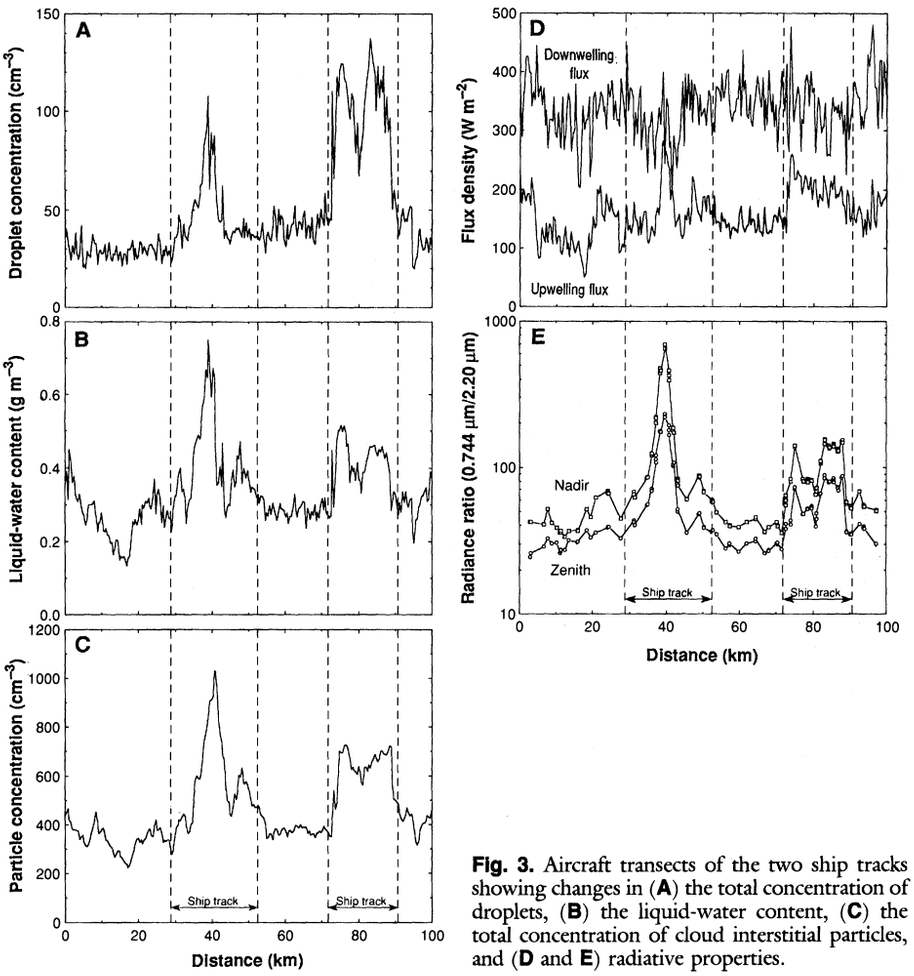

Fig. 3. Aircraft transects of the two ship tracks showing changes in (**A**) the total concentration of droplets, (**B**) the liquid-water content, (**C**) the total concentration of cloud interstitial particles, and (**D** and **E**) radiative properties.

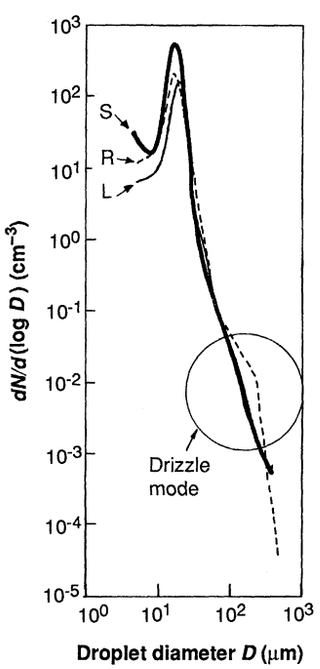

Fig. 4. The droplet size distribution in the first ship track (S) and on either side (L, R) of this track. Note the absence of a strong drizzle mode in the ship track cloud compared to the adjacent region R.

tracks. The differences in the total concentrations of droplets and particles between the first and second ship tracks suggest that the first track was younger than the second track. The higher total concentrations of particles and the lower concentrations of cloud droplets in the first track suggest that there was a temporal conversion of Aitken nuclei to CCN to droplets. Such a conversion provides an explanation for the longevity of ship tracks. The tracks will tend to persist until the total particles and trace gases are significantly depleted.

A puzzling feature of our aircraft observations is that the liquid-water content is higher in the ship track (Fig. 3B) than in the surrounding cloud. This observation prompted speculation that the release of heat and moisture from ships might produce dynamical effects on clouds that increase their liquid-water content (*17*). However, in a subsequent analysis, Albrecht showed that the liquid-water content of marine stratocumulus clouds was substantially less than the adiabatic value while similarly appearing clouds that developed in admixtures of marine and polluted continental air had, in general, close to adiabatic liquid-water contents (*18*). The comparatively higher droplet concentrations in the clouds affected by continental air evidently caused this difference. High droplet concentrations and hence small mean radii suppress the growth of large droplets by collision (through a collision efficiency threshold); in turn, the development of drizzle is suppressed. Thus, "clean" marine stratocumulus clouds are more likely to lose liquid water through precipitation. Clearly, a similar phenomenon could account for the higher liquid-water contents in the ship tracks.

To test this hypothesis, we averaged the droplet-size distribution across the first ship track and compared it with equal distances of cloud on either side of the ship track (Fig. 4). The concentration of droplets of diameter >200 μm (the usually accepted minimum size for drizzle) in the ship track was only about one-tenth of that in the surrounding cloud. The largest droplet found in the ship track was 800 μm, whereas some drops in the cloud unaffected by the ship track were 1200 μm in diameter. We conclude that the liquid water content in the ship tracks was higher because the higher droplet concentration and the smaller average droplet sizes restricted loss of liquid water by precipitation.

REFERENCES AND NOTES

1. P. Squires, *Tellus* **8**, 443 (1956); *ibid.* **10**, 256 (1958); S. Twomey and J. Warner, *J. Atmos. Sci.* **24**, 702 (1967).
2. S. Twomey and T. A. Wojciechowski, *J. Atmos. Sci.* **26**, 684 (1969); P. Squires, *J. Rech. Atmos.* **2**, 197 (1966); L. F. Radke and P. V. Hobbs, *Science* **193**, 999 (1976).
3. S. A. Twomey, M. Piepgrass, T. L. Wolfe, *Tellus* **36B**, 356 (1984); R. J. Charlson, J. E. Lovelock, M. O. Andreae, S. G. Warren, *Nature* **326**, 655 (1987).
4. S. Twomey, *Atmos. Environ.* **8**, 1251 (1974); L. F. Radke, in *Symposium on the Role of Clouds in Atmospheric Chemistry and Global Climate*, Anaheim, CA, 30 January to 3 February 1989 (American Meteorological Society, Boston, 1989), pp. 310–315.
5. J. H. Conover, *J. Atmos. Sci.* **23**, 778 (1966); S. Twomey, *ibid.* **25**, 333 (1968).
6. J. A. Coakley, Jr., R. L. Bernstein, P. A. Durkee, *Science* **237**, 1020 (1987).
7. For an overview of FIRE [First ISCCP (International Satellite Cloud Climatology Project) Regional Experiment] see S. K. Cox, D. S. McDougal, D. A. Randall, R. A. Schiffer, *Bull. Am. Meteorol. Soc.* **68**, 114 (1987). For an overview of the marine stratocumulus component of the experiment see B. A. Albrecht, D. A. Randall, S. Nicholls, *ibid.* **69**, 618 (1988).
8. S. Twomey, *Atmospheric Aerosols* (Elsevier, New York, 1977).
9. Cloud condensation nuclei serve as the particles on which cloud droplets condense when they are exposed to water supersaturations of less than a few percent. They are a subset of the total particle population.
10. L. F. Radke, in *Precipitation Scavenging, Dry Deposition, and Resuspension*, H. R. Pruppacher, R. G. Semonim, W. G. N. Slinn, Eds. (Elsevier, New York, 1983), pp. 71–78.
11. M. D. King, M. G. Strange, P. Leone, L. R. Blaine, *J. Atmos. Oceanic Technol.* **3**, 513 (1986).
12. At the shortest wavelengths, the absorption of solar radiation by the cloud is negligible; therefore, an increase of optical thickness leads to an increase in

the upwelling radiation at all levels in the deep interior of a cloud. In the near-infrared, on the other hand, the increased optical thickness leads to a reduction in the upwelling radiance in the middle of a cloud at wavelengths where the absorption of solar radiation by water droplets is significant.
13. For typical maritime conditions, the droplet concentration is $N \propto C^{0.8}$, where C is the CCN concentration at 1% supersaturation. Thus an increase of 80 drops per cubic centimeter would require approximately 240 CCN per cubic centimeter, which is consistent with the measurements in Fig. 3C; see S. Twomey, *J. Phys. Chem.* **84**, 1459 (1980).
14. L. F. Radke, S. K. Domonkos, P. V. Hobbs, *J. Rech. Atmos.* **15**, 225 (1981).
15. J. Hallet and J. Hudson, *Aerosol Sci. Technol.* **10**, 70 (1989).
16. P. V. Hobbs, J. L. Stith, L. F. Radke, *J. Appl. Meteorol.* **19**, 439 (1980); R. F. Pueschel, E. W. Barrett, D. L. Wellman, J. A. McGuire, *Geophys. Res. Lett.* **8**, 221 (1981).
17. L. F. Radke, J. H. Lyons, P. V. Hobbs, J. A. Coakley, *Proceedings of the 10th International Cloud Physics Conference*, Bad Homburg, Federal Republic of Germany, 15 to 20 August 1988 (Deutscher Wetterdienst, Offenbach am Main, FRG, 1988), pp. 121–123; W. M. Porch, C. J. Kao, T. G. Kyle, R. G. Kelley, in *Symposium on the Role of Clouds in Atmospheric Chemistry and Global Climate*, Anaheim, CA, 30 January to 3 February 1989 (American Meteorological Society, Boston, 1989), pp. 161–164.
18. B. A. Albrecht, *Science* **245**, 1227 (1989).
19. We thank P. V. Hobbs, P. A. Durkee, J. H. Lyons, and H. Terry for useful comments and contributions. The coordinating role of the FIRE science team is gratefully acknowledged. This work was supported in part by National Science Foundation grant ATM-8615344 (L.F.R. and M.D.K.) and National Aeronautics and Space Administration grant NAG-1-935 (J.A.C.)

26 June 1989; accepted 2 October 1989

Structure of Complex of Synthetic HIV-1 Protease with a Substrate-Based Inhibitor at 2.3 Å Resolution

MARIA MILLER, JENS SCHNEIDER, BANGALORE K. SATHYANARAYANA, MIHALY V. TOTH, GARLAND R. MARSHALL, LEIGH CLAWSON, LINDA SELK, STEPHEN B. H. KENT,*† ALEXANDER WLODAWER†

The structure of a complex between a peptide inhibitor with the sequence *N*-acetyl-Thr-Ile-Nle-Ψ[CH_2-NH]-Nle-Gln-Arg.amide (Nle, norleucine) with chemically synthesized HIV-1 (human immunodeficiency virus 1) protease was determined at 2.3 Å resolution (*R* factor of 0.176). Despite the symmetric nature of the unliganded enzyme, the asymmetric inhibitor lies in a single orientation and makes extensive interactions at the interface between the two subunits of the homodimeric protein. Compared with the unliganded enzyme, the protein molecule underwent substantial changes, particularly in an extended region corresponding to the "flaps" (residues 35 to 57 in each chain), where backbone movements as large as 7 Å are observed.

RETROVIRAL PROTEASES, WHICH are members of the aspartic protease family, specifically process high molecular weight viral polyproteins into individual structural proteins and enzymes (*1*). Mutation of the active site Asp to Asn in HIV-1 protease (HIV-1 PR) prevents processing of polyprotein (*2*), so that immature, noninfective virions result. Thus specific inhibitors of HIV-1 PR would serve as candidates for AIDS therapeutics.

The structure of cloned HIV-1 PR has been determined at 3 Å (*3*). Important corrections were made in a 2.8 Å x-ray study with synthetic HIV-1 PR (*4*) and have been confirmed for the cloned material (*5*). More detailed information needed for inhibitor design can be gleaned from studies of enzymes complexed with substrate-derived inhibitors. For cellular aspartic proteases, extensive investigation of inhibitor complexes with endothiapepsin (*6*), rhizopuspepsin (*7*), and penicillopepsin (*8*) have been reported.

Modeling of the interaction of inhibitors and substrates with HIV-1 PR (*9*) could only make limited predictions in the absence of experimental data, and the available crystal form of the HIV-1 PR was not suitable for inhibitor studies because of the presence of only one subunit (one-half of the molecule) in the asymmetric unit and the limited diffraction (*3–5*). For these reasons we cocrystallized HIV-1 PR with a substrate-based inhibitor.

An inhibitor was designed based on the sequence of a good peptide substrate for the enzyme. Hexapeptides derived from known cleavage sites of the viral *gag-pol* polyprotein products were synthesized, and several were shown to be substrates (*10*). The hexapeptide substrate with the lowest Michaelis constant K_m (1.4 m*M*), Ac-Thr-Ile-Met-Met-Gln-Arg.amide (where the amide is on the carboxyl terminus), was chosen as a candidate for further modification. The isosteric amino acid norleucine (Nle), in which the sulfur of the Met side chain is replaced by a methylene group, was used for synthetic simplification and shown to give a substrate, Ac-Thr-Ile-Nle-Nle-Gln-Arg.amide, with comparable affinity. In an approach analogous to that of Szelke *et al.* (*11*) for human renin, we prepared an inhibition of HIV-1 PR, compound MVT-101, with the sequence *N*-acetyl-Thr-Ile-Nle-Ψ[CH_2-NH]-Nle-Gln-Arg.amide (*12*), where the scissile peptide bond has been replaced by a reduced analog (*13,14*).

The crystal structure of the complex was solved by molecular replacement using the native HIV-1 PR (*4*) as a starting model (*15*). The $|F_o - F_c|\alpha_c$ map based on the phases from the preliminary refinement showed density in the active site corresponding to the inhibitor. A model of the hexapeptide with a reduced peptide bond was fitted easily, with the polarity indicated primarily by the bulky side chain of Arg^{206}. The positions of all six residues of the inhibitor are well defined by the electron density (Fig. 1). The inhibitor binds to the

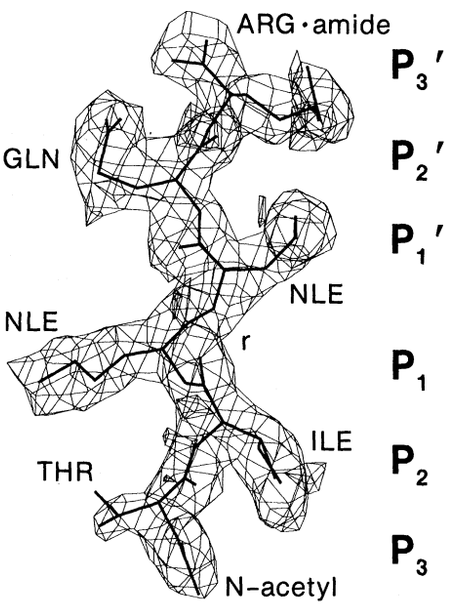

Fig. 1. A view of the electron density and of the final atomic model of the inhibitor MVT-101. This $|2F_o - F_c|\alpha_c$ electron density map was calculated after refinement and was contoured at the 0.8σ level. All of the atoms belonging to the inhibitor molecule, with the exception of Cγ of Thr^{201}, are in the density.

M. Miller, B. K. Sathyanarayana, A. Wlodawer, Crystallography Laboratory, NCI–Frederick Cancer Research Facility, BRI-Basic Research Program, P.O. Box B, Frederick, MD 21701.
J. Schneider, L. Clawson, L. Selk, S. B. H. Kent, Division of Biology, California Institute of Technology, Pasadena, CA 91125.
M. V. Toth and G. R. Marshall, Department of Pharmacology, Washington University School of Medicine, St. Louis, MO 63110.

*Current address: Graduate School of Science and Technology, Bond University, Queensland, Australia 4229.
†To whom correspondence should be addressed.